P528 Notes #10: QCD at High Energies

David Morrissey
March 30, 2021

A key feature of Quantum Chromodynamics (QCD) that the effective strength of the strong gauge coupling factor α_s depends on the energy scale at which it is measured; it is large at low energies but grows smaller at high energies. For processes with characteristic momentum much larger than $\Lambda_{QCD} \simeq 200$ MeV, the QCD gauge coupling is small enough that processes in the theory can computed reliably in perturbation theory. Even so, the low-energy dynamics of QCD that lead to confinement must still accounted for if one wants to compare the predictions of high-energy QCD to experimental data [1, 2, 3, 4].

In this context, QCD confinement enters in two ways. First, when QCD-charged objects such as quarks and gluons are created in high-energy collisions, they must eventually arrange themselves into colour-neutral objects since we never observe them in isolation. This occurs through a process of sequential radiation called *showering*, followed by *hadronization* into a collection of hadrons. The net effect is that final-state quarks and gluons are reprocessed into collimated *jets* of colour-singlet hadrons.

The second appearance of confinement in high-energy collisions comes from hadronic initial states. We are not able to arrange collisions of individual quarks or gluons with each other, but we can and do set up collisions of hadronic objects made of them, such as protons. For example, the LHC collides two beams of protons at centre-of-mass (CM) energies approaching $\sqrt{s} = 14$ TeV. It turns out that a significant fraction of such collisions can be treated as occuring between the quark or gluon *parton* constituents of the colliding hadrons.

In these notes we give a brief overview of how these processes take place and the methods that are used to compute them. A recurring theme will be *factorization*, which implies that the perturbative high-energy *hard* parts of the collision can be treated mostly independently of the non-perturbative low-energy *soft* portions. This splitting is linked to the asymptotic freedom of QCD and the infrared behaviour of quantum field theories.

1 Creating QCD Stuff: Jets

Let us begin with the creation of quarks and gluons in energetic collisions of uncoloured particles such as electrons.

1.1 $e^+e^- \to$ hadrons

An important process for testing QCD as the theory of the strong force is $e^+e^- \to$ hadrons, in which an electron and a positron are smashed together in their CM frame with $\sqrt{s} = \sqrt{(p_1 + p_2)^2} \gg 1$ GeV. The corresponding ratio of cross sections $R(s) = \sigma(e^+e^- \to \text{hadrons})/\sigma(e^+e^- \to \mu^+\mu^-)$ for all observed hadronic final states relative to muons is shown

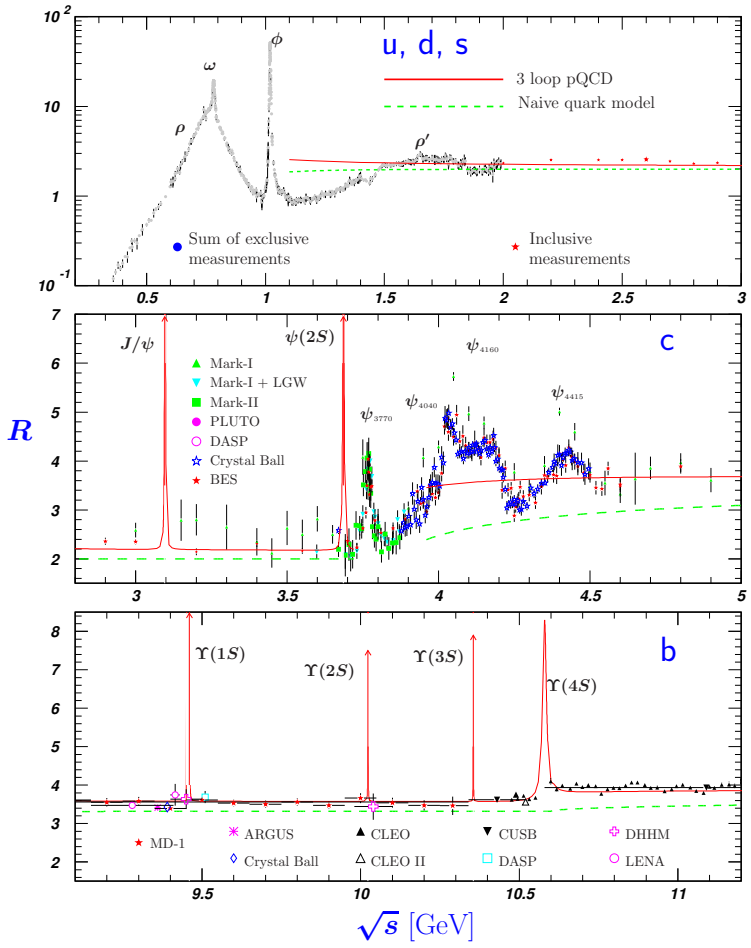

Figure 1: Observed ratios of $R(s) = \sigma(e^+e^- \to \text{hadrons})/\sigma(e^+e^- \to \mu^+\mu^-)$ compared with predictions of the quark model, from Ref. [5].

in Fig. 1, taken from Ref. [5]. This is the same plot as shown in `notes-08`, but now zoomed in over various energy ranges near quark mass thresholds.

Let us now compare the data for $R(s)$ to a calculation of quark production in $e^+e^- \to q\bar{q}$. At leading order, the matrix element gets contributions from diagrams with a photon or a Z^0 in the s-channel, with the photon diagram dominating for $\sqrt{s} \ll m_Z$. Arranging this into a cross section and taking the ratio to the corresponding muon process, the result for $\sqrt{s} > 2m_s$ is

$$\begin{aligned} R_{qq}(s) &:= \frac{\sigma(e^-e^+ \to q\bar{q})}{\sigma(e^-e^+ \to \mu^-\mu^+)} \\ &\simeq N_c \left[\left(\frac{2}{3}\right)^2 + \left(\frac{-1}{3}\right)^2 + \left(\frac{-1}{3}\right)^2 + \theta_c \left(\frac{2}{3}\right)^2 + \theta_b \left(\frac{-1}{3}\right)^2 + \theta_t \left(\frac{2}{3}\right)^2 \right] \\ &= \left(\frac{6 + 4\theta_c + \theta_b + 4\theta_t}{9} \right) N_c \ , \end{aligned} \tag{1}$$

where $N_c = 3$ is the number of colours and $\theta_f = \Theta(\sqrt{s} - 2m_f)$. The terms in this expression come from u, d, s, c, b, and t quarks respectively, and it matches the data quite well for $\sqrt{s} \gtrsim 2$ GeV and away from mass thresholds. In particular, the result of Eq. (1) corresponds to the dashed green line in Fig. 1. When the calculation is extended to higher orders in perturbative QCD, the agreement is even better as shown by the red line in Fig. 1.

The experimental success of Eq. (1) suggests that identifying the cross section for producing quarks and gluons with the physical production of hadrons is a sensible thing to do. However, the particles seen in the final state are not quarks or gluons, but rather collections of many hadrons (in the form of mesons and baryons). It is not immediately obvious how to get such collections of hadrons from high-energy quarks or gluons.

1.2 Jets

A clue for how to explain this result is the observation that the hadronic products of e^+e^- collisions with $\sqrt{s} \gg \Lambda_{QCD}$ usually consist of two distinct back-to-back *jets*, each consisting of a collection of highly collimated mesons and baryons. Summing over all their constituents, the net momentum distribution of these jets usually agrees very well with the expected momentum distribution for a pair of quarks emitted in $e^+e^- \to q\bar{q}$. This suggests that each high-energy quark produced in the collision typically leads to a jet. A further piece of evidence for this picture is that the probability to see three energetic jets in the final state coincides well with the probability to radiate an energetic gluon from one of the quark legs.

The formation of QCD jets makes sense from the point of view of asymptotic freedom. The $q\bar{q}$ pair produced has no net colour, and the quark and anti-quark retain a *colour connection* in the form of virtual gluons and $q\bar{q}$ pairs. However, for quarks produced with relative momenta well above Λ_{QCD}, these *soft* exchanges are incapable of transferring large amounts of momentum on the order of the underlying high-energy $e^+e^- \to q\bar{q}$ *hard* collision. Heuristically, each soft exchange takes time Λ_{QCD}^{-1}, and transfers momentum Λ_{QCD}. This is much slower than the time scale for the energetic quarks to separate beyond the range of these soft exchanges, also on the order Λ_{QCD}^{-1}, and there is not enough time to exchange a significant amount of momentum.

As each quark travels along, it radiates soft or collinear gluons which in turn split into more gluons and $q\bar{q}$ pairs. This is called a *parton shower*. The probability for each emission is governed by $\alpha_s(p_T)$ (and logarithmic enhancements), where p_T is the momentum of the emitted state transverse to the direction of the initial quark (or gluon). Asymptotic freedom thus favours low-p_T radiation. The constituents of such a shower therefore tend to travel along together provided the initial momentum of the hard quark (or gluon) is much greater than the typical transverse momenta $p_T \sim \Lambda_{QCD}$ of the radiated particles. These roughly collinear QCD states subsequently attract and bind to form hadrons in a process called *hadronization*. Both the parton shower and hadronization are non-perturbative processes in QCD. There exist a number of phenomenological models for them, with the best-known implementations encoded within the PYTHIA [6] and HERWIG [7] computer programs.

The essential point that allows us to make perturbative predictions for QCD processes

is that the hard and soft dynamics factorize. Starting from the hard quark or gluon-level matrix element, the kinematics of the outgoing jets are set almost entirely by the momenta of the energetic quarks and gluons that give rise to them. Non-perturbative QCD effects mainly dress up these final states into collimated jets of colour-singlet hadrons. In fact, this is not so different from QED. For example, in $e^+e^- \to \mu^+\mu^-$ the electromagnetic interaction between the outgoing muons does have much of an effect on their final momenta for $\sqrt{s} \gg 2m_\mu$. In contrast, for $\sqrt{s} \simeq 2m_\mu$ this interaction does become important and sometimes the outgoing muons even bind together to form *muonium*. Analogous quark-antiquark bound states are observed in Fig. 1 near quark mass thresholds. Furthermore, what we observe as a "muon" also typically includes a number of soft and collinear photons emitted as radiation that physical particle detectors are not able to resolve.

2 Making Stuff from QCD: Partons

Our modern understanding of hadrons is that they are bound states of quarks and gluons. A natural question to ask, then, is what happens when hadrons undergo high-energy collisions. In many cases, the results of such collisions can be understood in terms of a set of constituent *partons* that we identify (loosely) with quarks and gluons.

2.1 Deep Inelastic Scattering and the Parton Model

Much of what we know about the structure of protons (and neutrons) comes from deep inelastic scattering (DIS). In DIS, an energetic beam of leptons is shot into a thin target of of nucleons. The leptons scatter off the nucleons, and the momentum of the outgoing scattered leptons is measured. A specific example is $e^- p \to e^- X$, where X is an unspecified (and often unmeasured) hadronic final state. Hard scattering, with momentum transfer $|q^2| \gg \Lambda_{QCD}$, can be understood in terms of the electron scattering off one of the quarks in the proton through the exchange of a photon (or Z^0), as illustrated in Fig. 2. To relate theory to data we must do two things: i) calculate the electron-quark scattering matrix element; ii) relate this matrix element to the quark content of the proton.

The first step is straightforward and something we know how to do. Consider the process $e^-(k)\, q_i(p) \to e^-(k')\, q_i(p')$. Working in the quark-electron CM frame, we have

$$\frac{d\hat{\sigma}}{d\hat{t}} = \frac{2\pi\alpha^2 Q_i^2}{\hat{s}^2}\left[\frac{\hat{s}^2 + (\hat{s}+\hat{t})^2}{\hat{t}^2}\right] , \tag{2}$$

where Q_i is the electric charge of the quark, and $\hat{s}$ and $\hat{t}$ are the quark-electron system Mandelstam variables:

$$\hat{s} = (k+p)^2, \qquad \hat{t} = (k-k')^2 . \tag{3}$$

The net electron momentum transferred in the event is $q = (k' - k)$. Since the Lorentz-invariant q^2 is spacelike, it is standard to define the related positive quantity $Q^2 = -q^2$.

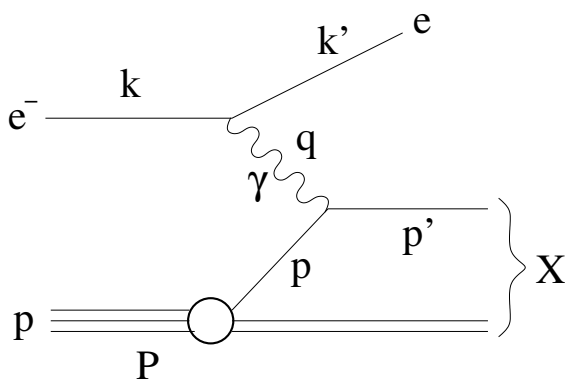

Figure 2: Deep inelastic scattering.

To relate this perturbative quark-level scattering cross section to the underlying electron-proton cross section, as measured in the lab frame where the proton is essentially at rest, we must specify how likely it is to get the quark species q_i from the proton with the given initial momentum. This is not something that can be done in perturbation theory. Instead, the QCD features of confinement and asymptotic freedom suggest a phenomenological *parton model* that is found to give an excellent descripton of data.

The main features of the parton model are [1, 3]:

- Hadrons consist of quarks (and anti-quarks) and gluons that are collectively called *partons*. They are typically treated as being massless.
- The partons move along with the parent hadron with momentum components transverse to the direction of the parent smaller than the QCD scale: $p_T \lesssim \Lambda_{QCD}$.
- The momentum of the parent hadron is carried collectively by the constituent partons. If P is the momentum of the parent, each constituent parton carries (longitudinal) momentum $p_i = x_i P$ with $0 < x_i < 1$.
- The probability density that a parton of species i carries momentum fraction x is given by the *parton distribution function* (PDF) $f_i(x)$.

With these properties, it follows that the total cross section for a high-energy process involving a hadron N in the initial state $A + N \to B + C$ is:

$$\sigma_{tot} = \sum_i \int dx \; f_i^N(x) \, \hat{\sigma}(A + q_i(xP) \to B + C) \; , \tag{4}$$

where the sum runs over all the partonic constituents of the hadron and $\hat{\sigma}$ is the parton-level cross section. The essential feature of the parton model is that it leads to a factorization of the perturbative hard parton-level matrix element and the non-perturbative dynamics embodied in the PDFs.

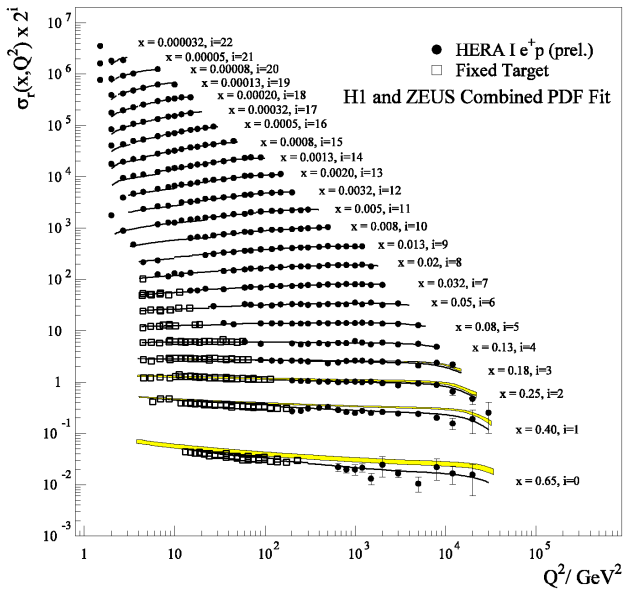

Figure 3: Predictions for deep inelastic scattering compared to data.

The PDFs in the parton model are universal (for a given hadron species). Parton densities are included for u, d, s, c, b, their anti-particles, and the gluon. They satisfy various sum rules such as

$$\int_0^1 dx \ \left[f_u^N(x) - f_{\bar{u}}^N(x)\right] = \begin{cases} 2; & N = p \\ 1; & N = n \end{cases} \tag{5}$$

$$f_u^p(x) = f_{\bar{u}}^{\bar{p}}(x) \tag{6}$$

$$1 = \int_0^1 dx \sum_i f_i(x) x \tag{7}$$

The first two results reflect the net quark content of the nucleons while the third sum rule corresponds to the partons carrying the momentum of the parent hadron. Some popular sets of PDFs are CTEQ [8], MRST [9], and NNPDF [10].

Going back to DIS, it is possible to relate the parton momentum fraction x in each event to observables in that event. Treating all the constituents as massless, a good approximation for $\hat{s} \gg \Lambda_{QCD}$, we have

$$\hat{s} = (k+p)^2 = 2k{\cdot}p = 2x\, k{\cdot}P = x(k+P)^2 = x\, s \tag{8}$$

where s is the electron-proton system Mandelstam variable. We also have

$$0 = p'^2 = (p+q)^2 = 2x\, P{\cdot}q - Q^2 \qquad \Rightarrow \qquad x = \frac{Q^2}{2P{\cdot}q} \tag{9}$$

where the first condition comes from the relative masslessness of the outgoing quark.

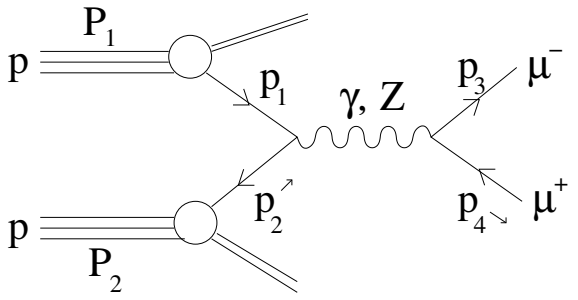

Figure 4: Drell-Yan production of $\mu^+\mu^-$ in a pp collision.

Applying the parton model to DIS and using the parton-level cross section given in Eq. (2) (with a change of variables), we find

$$\frac{d^2\sigma}{dxdQ^2} = \sum_i f(x)\, Q_i^2 \left\{ \frac{2\pi\alpha^2}{Q^4} \left[1 + \left(1 - \frac{Q^2}{xs} \right) \right] \right\} \ , \tag{10}$$

where Q_i is the electric charge of the i-th parton (not to be confused with the momentum transfer variable Q^2). Note that all the kinematic dependence is contained within the curly braces, while the first factor (outside the braces) depends on x alone. This result is known as *Bjorken scaling*. It receives controlled corrections at higher orders in QCD. In Fig. 3 we show the predictions of the parton model for DIS (with QCD corrections) along with some experimental data – evidently the theory does very well over many orders of magnitude. While this result is specific to $e^- p \to e^- X$, DIS can also be performed using a neutron target or through the W-mediated process $\bar{\nu}_\ell\, p \to \ell^- X$.

2.2 Drell-Yan

The Drell-Yan process is electroweak production of a lepton pair from a hadronic initial state. We show an example of Drell-Yan in Fig. 4. The lab frame typically coincides with the centre-of-mass (CM) frame of the pair of colliding hadrons. The remnants of the protons not involved in the hard collision are relatively collinear with the collider beam and are not usually seen.

Following the parton model, the total cross-section for the Drell-Yan process $pp \to \ell^+\ell^-$ is (at leading order)

$$\sigma(pp \to \ell^+\ell^-) = \sum_{ij} \int dx_1 \int dx_2 \; f_i^p(x_1) f_j^p(x_2)\, \hat{\sigma}(q_i(p_1)\bar{q}_i(p_2) \to \ell^-\ell^+) \ , \tag{11}$$

where $p_1 = x_1 P_1$ and $p_2 = x_2 P_2$. In the pp CM frame,

$$p_1 = x_1(E, 0, 0, E) \ , \qquad p_2 = x_2(E, 0, 0, -E) \ , \tag{12}$$

where we have taken the z axis along the direction of the beam. From these expressions we see that the parton-level Mandelstam variable $\hat{s}$ is related to the lab-frame Mandelstam

variable s by

$$\hat{s} = (p_1 + p_2)^2 = 2x_1x_2\, P_1 \cdot P_2 = x_1x_2\, s\ . \tag{13}$$

Note also that even though the collision is taking place in the pp CM frame, this does not coincide in general with the CM frame of the colliding partons. Instead, the parton CM frame has a net boost along the beam direction relative to the lab frame corresponding to the longitudinal momentum $(x_1 - x_2)\sqrt{s}/2$. This makes the kinematics of events at colliders more difficult to reconstruct than if the initial states were fundamental (as opposed to composite) particles. In many cases we focus entirely on the *transverse* momentum $\vec{p}_T$ of the particles that are produced, where $\vec{p}_T$ is the component of a particle's momentum orthogonal (or transverse) to the beam direction.

Historically, DIS has been used to determine parton distribution functions. Since the same PDFs apply to other processes such as Drell-Yan, we can use the measured PDFs from DIS to make predictions for Drell-Yan and other cross-sections.

2.3 Parton Evolution

Going beyond the leading order (LO), one encounters an additional complication when dealing with partons. At the next-to-leading order (NLO) and beyond (N^nLO), the PDFs pick up a dependence on a new dimensionful scale μ_F that we usually identify with the typical momentum scale of the underlying hard process, $\mu_F^2 \sim Q^2$. This scale μ_F is called the *factorization scale*, and it corresponds to where we choose to split up the dynamics of process into soft (low-energy and non-perturbative) and hard (high-energy and perturbative) pieces.

To see how this works, consider the NLO correction to the Drell-Yan process in which a gluon is radiated off one of the initial quark legs. If perturbation theory is to be applicable, the probability to radiate such a gluon should be small in some sense. Computing the correction to the hard matrix element from radiating a gluon with transverse momentum p_T, the correction to the hard matrix element goes like

$$\frac{d(\Delta\hat{\sigma})}{dp_T} \sim \frac{\alpha_s(p_T)}{p_T}\hat{\sigma}\ . \tag{14}$$

For large p_T we see that this correction is reasonable, being suppressed by both the large p_T and the perturbatively small $\alpha_s(p_T)$. However, for small $p_T \sim \Lambda_{QCD}$, the correction becomes very large since α_s blows up and the denominator becomes small. This would seem to invalidate our use of perturbation theory, even though the energy of the underlying Drell-Yan process is much larger than Λ_{QCD}.

This might look bad, but there is a way out. Note that the problem arises when the gluon emitted is either very soft or is collinear with the beam. In both cases, for $p_T \lesssim \Lambda_{QCD}$ the gluon continues to travel along with the incident hadron and can't be said to escape as an observable particle (or as well see below, a jet of particles). It is therefore sensible to

include the effects of soft and collinear gluon (or quark) radiation within the PDFs since it is effectively just modifying the parton content of the initial state.

In contrast to the case of soft gluons, a gluon emitted with large $p_T \gg \Lambda_{QCD}$ is expected to escape from the hadron and lead to an additional observable particle in the final state. Clearly we do not want to include these hard emissions within the PDFs. Instead, we should keep them as perturbative corrections to the parton-level hard matrix element. More generally, this leads to the question of what p_T value one should use to divide between soft radiation that is included within the PDFs and hard radiation that is handled as a perturbative correction to the parton-level matrix elements. The answer is μ_F, the factorization scale, which represents the dividing line between PDFs and matrix elements. We can choose μ_F any way we like, but a judicious choice will help us optimize the perturbative expansion of the hard matrix elements. This best choice is usually $\mu_F^2 \sim Q^2$, the typical large momentum scale associated with the underlying LO hard process.

Different choices of the factorization scale lead to different sets of PDFs that incorporate varying amounts of NLO (and beyond) parton radiation. We therefore write $f_i(x, \mu_F)$ to account for this property. Even though the PDFs are inherently non-perturbative, it is possible to relate PDF sets at different values of μ_F ($\gg \Lambda_{QCD}$) using perturbation theory. The result is described by the DGLAP[1] equations:

$$\begin{aligned}
\frac{df_g(x,\mu_F)}{dt_F} &= \frac{\alpha_s(\mu_F)}{\pi}\int_x^1 \frac{dz}{z}\left(P_{g\to g}(z) f_g(\frac{x}{z},\mu_F) + P_{q\to g}(z)\sum_q \left[f_{q\to g}(\frac{x}{z},\mu_F) + f_{\bar{q}\to g}(\frac{x}{z},\mu_F)\right]\right) , \\
\frac{df_q(x,\mu_F)}{dt_F} &= \frac{\alpha_s(\mu_F)}{\pi}\int_x^1 \frac{dz}{z}\left[P_{q\to q}(z) f_q(\frac{x}{z},\mu_F) + P_{g\to q}(z) f_g(\frac{x}{z},\mu_F)\right] .
\end{aligned} \tag{15}$$

Here, $t_F = \ln(\mu_F)$, while $P_{g\to g}$, $P_{q\to q}$, $P_{q\to g}$, and $P_{g\to q}$ are called splitting functions. They can be computed in perturbation theory (for $\mu_F \gg \Lambda_{QCD}$). For example, $P_{g\to g}$ corresponds to diagrams in which a gluon splits into a gluon and something else, while $P_{g\to q}$ corresponds to diagrams where a gluon splits into the quark q and anything else.

References

[1] M. E. Peskin and D. V. Schroeder, "An Introduction To Quantum Field Theory," *Reading, USA: Addison-Wesley (1995) 842 p*

[2] S. Pokorski, "Gauge Field Theories," *Cambridge, UK: Cambridge U. Press (2000) 609p*

[3] R. K. Ellis, W. J. Stirling and B. R. Webber, "QCD and collider physics," Camb. Monogr. Part. Phys. Nucl. Phys. Cosmol. **8**, 1 (1996).

[4] M.E. Peskin, "Concepts of Elementary Particle Physics," https://www.slac.stanford.edu/ mpeskin/Physics152/theBook.pdf

[1] DGLAP = Dokshitzer, Gribov, Lipatov, Altarelli, and Parisi.

[5] C. Patrignani *et al.* [Particle Data Group], "Review of Particle Physics," Chin. Phys. C **40**, no. 10, 100001 (2016);
http://pdg.lbl.gov/

[6] T. Sjostrand, S. Mrenna, P. Z. Skands, "PYTHIA 6.4 Physics and Manual," JHEP **0605**, 026 (2006). [hep-ph/0603175],
http://home.thep.lu.se/ torbjorn/Pythia.html

[7] M. Bahr, S. Gieseke, M. A. Gigg, D. Grellscheid, K. Hamilton, O. Latunde-Dada, S. Platzer, P. Richardson *et al.*, "Herwig++ Physics and Manual," Eur. Phys. J. **C58**, 639-707 (2008). [arXiv:0803.0883 [hep-ph]].

[8] S. Dulat *et al.*, "New parton distribution functions from a global analysis of quantum chromodynamics," Phys. Rev. D **93**, no. 3, 033006 (2016) [arXiv:1506.07443 [hep-ph]],
http://www.physics.smu.edu/scalise/cteq/

[9] A. D. Martin, W. J. Stirling, R. S. Thorne and G. Watt, "Parton distributions for the LHC," Eur. Phys. J. C **63**, 189 (2009) [arXiv:0901.0002 [hep-ph]],
https://mstwpdf.hepforge.org/

[10] R. D. Ball *et al.* [NNPDF Collaboration], "Parton distributions for the LHC Run II," JHEP **1504**, 040 (2015) [arXiv:1410.8849 [hep-ph]],
https://nnpdf.hepforge.org/